Journal of Power Sources 196 (2011) 4719–4723

Contents lists available at ScienceDirect

Journal of Power Sources

journal homepage: www.elsevier.com/locate/jpowsour

Short communication

Effect of gas flow rates and Boudouard reactions on the performance of Ni/YSZ anode supported solid oxide fuel cells with solid carbon fuels

Andrew C. Chien, Steven S.C. Chuang*

Department of Chemical and Biomolecular Engineering, FirstEnergy Advanced Energy Research Center, The University of Akron, 200 E Buchtel Commons, Akron, OH 44325-3906, United States

ARTICLE INFO

Article history:
Received 30 November 2010
Received in revised form
28 December 2010
Accepted 7 January 2011
Available online 19 January 2011

Keywords:
Boudouard reaction
Solid oxide fuel cells
Coconut coke
Oxidation of solid carbon
Pulse transient studies

ABSTRACT

The effects of carrier gas flow rates and Boudouard reaction on the performance of Ni/YSZ anode-supported solid oxide fuel cells (SOFCs) have been studied with coconut coke fuels at 800 °C. Decreasing flow rates of carrier gas from 1000 to 50 ml min^{-1} increased open circuit voltages and current densities from 0.71 to 0.87 V and from 0.12 to 0.34 A cm^{-2}, respectively. The increased cell performance was attributed to the increasing extent of electrochemical oxidation of CO, a product of Boudouard reaction. The contribution of CO oxidation to current generation was estimated to 66% in flowing inert carrier gas at 50 ml min^{-1}. The pulse transient studies confirmed the effect of flow rates on cell performance and also revealed that CO and CO_2 can displace adsorbed hydrogen on carbon fuels. Flowing CO_2 over coconut coke fuel produced CO via Boudouard reaction. The presence of CO led to a highest power density of 95 mW cm^{-2}, followed by a concurrent decline of power density and CO concentration. The declined power density along with decreasing CO concentration further verified contribution of gaseous CO to the power generation of C-SOFC; the decreasing CO concentration showed a typical kinetics behavior of Boudouard reaction, suggesting the loss of active sites on carbon surface for the reaction.

1. Introduction

Direct utilization of solid carbon in fuel cells has attracted increasing attention because of its high thermodynamic efficiency [1,2]. The electrical efficiency of direct carbon fuel cells (DCFCs) can reach up to 100% compared with 30–40% of traditional coal-fired power plants [3,4]. DCFCs produce high concentration of carbon dioxide which can be sequestrated without expensive separation and purification steps. DCFCs operate by electrochemical oxidation of carbon in the absence of nitrogen, minimizing NO_x emission without costly selective reduction process commonly employed by coal-fired power plants.

DCFCs can be categorized by electrolytes into three types: (i) molten salts [1,5], (ii) solid electrolyte [6,7], and (iii) composite of molten salt and solid electrolyte [8,9]. Compared with molten salt electrolyte based fuel cells, solid oxide fuel cells (SOFCs) provide advantages of avoiding corrosion/degradation from liquid electrolyte and simplicity of stack assembly. The basic principle of carbon-based SOFCs (C-SOFCs) is electrochemical oxidation of solid carbon by oxygen anions (O^{2-}) on the anode. With proper anode catalysts, oxygen anion is expected to electrochemically oxidize any combustible substance such as H_2, CH_4, or coal. Despite the advantages of C-SOFCs, most reported C-SOFCs produced a power less than 100 mW cm^{-2} at 800 °C. The low C-SOFC performance could be attributed to limited contact of solid carbon at three phase boundary (TPB) of anodes and the low activity of the sites, where the catalytic electrochemical oxidation reaction occurs.

Although electrochemical oxidation of solid carbon is limited at TPB on the surface of the porous anode, oxidation products, i.e. CO and CO_2, can cause a significant contribution to electric power because (i) CO can be further electrochemically oxidized in the porous anode electrode to CO_2 and (ii) CO_2 can undergo Boudouard reaction leading to CO, as illustrated in Fig. 1. An approach to enhancing the performance of C-SOFCs is to directly introduce catalytic gasification of carbon by integrating Boudouard reaction with C-SOFCs [10,11]. The Boudouard reaction is highly endothermic ($\Delta H^\circ_{298\,K} = 172.5$ kJ mol^{-1}) and the required heat can be supplied from the exothermic carbon oxidation ($\Delta H^\circ_{298\,K} = 393.5$ kJ mol^{-1}). Hot CO_2 steam exiting from C-SOFCs can be recycled to the inlet stream, to further increase CO production for C-SOFCs.

The objective of this study is to determine the effect of gas flow rates and Boudouard reaction on cell performance of C-SOFCs. The results showed that low carrier gas flow rates increased residence time of CO, thereby increasing its contribution to current gener-

* Corresponding author. Tel.: +1 330 972 6993; fax: +1 330 972 5856.
E-mail address: schuang@uakron.edu (S.S.C. Chuang).

0378-7753/$ – see front matter © 2011 Elsevier B.V. All rights reserved.
doi:10.1016/j.jpowsour.2011.01.033

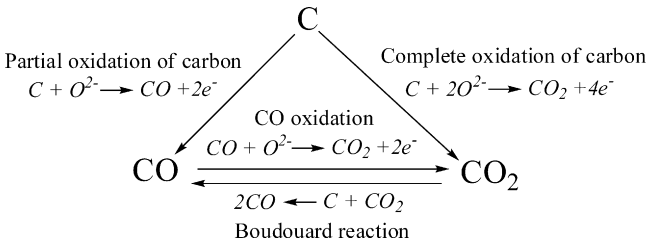

Fig. 1. Carbon oxidation, Boudouard reaction, and CO oxidation on C-SOFCs.

ation. Low carrier flow rate could also increase the production of CO from Boudouard reaction. The increase in current generation was further confirmed by CO and CO_2 step and pulse transient studies.

2. Experimental

2.1. Cell fabrication

The SOFC used in this study consisted of anode support, anode interlayer, electrolyte, cathode interlayer, and cathode, as shown in Fig. 2. The anode support (Ni/YSZ) (70/30 wt%), anode interlayer (Ni/YSZ) (50/50 wt%), and electrolyte (pure YSZ) were fabricated by tape casting. The Ni/YSZ slip was prepared by ball milling a mixture of NiO (Atlantic Equipment Engineers Inc.) and YSZ powder (Tosoh, 8 mol%), binders, dispersants and ethanol. The casted anode support, interlayer, and electrolyte tape were then attached together by spraying terpineol on each side of contact to form three-layer laminate. The laminate was cut in a circular form, uniaxially pressed under 10,000 psi, sintered at 1000 °C for 16 h and 1450 °C for 2 h. The circular cell disk was 2.5 cm in diameter and 700 μm thick. The cathode interlayer, YSZ/$La_{0.8}Sr_{0.2}MnO_3$ (LSM) (50/50 wt%, Heraeus), and cathode, pure LSM paste with an effective area of 1.5 cm^2 were subsequently screen-printed on the electrolyte side of the disk and fired at 1200 and 1100 °C, respectively, for 2 h.

2.2. Cell testing

Fig. 3a shows the schematic for C-SOFC testing, consisting of (i) a gas manifold for switching gas streams and adjusting gas flow rates and (ii) a cell-testing apparatus including coal injection, stainless chamber, and a furnace. The compositions of the anode compartment effluent were continuously monitored by a mass spectrometer (MS, Omnistar GSD 301). The mass/electron ratios (m/e) in MS were selected for H_2 (2), He (4), CH_4 (15), H_2O (18), CO (28), O_2 (32), and CO_2 (44). The gas compositions was also verified by a gas chromatographer (GC, SRI 3100) with a helium ionization detector (HID), which detected volatile inorganics such as H_2, N_2, O_2, CO, and CO_2. The open circuit voltage (OCV) and the cell voltage–current density–power density (V–I–P plot) were characterized by a Solartron potentiostat (Cell test system 1470 E). The V–I–P plot was recorded at 60 scans min^{-1} from the OCV to zero in a voltage control mode. The C-SOFC performance was measured at open circuit by galvanic control or close (i.e. electrochemical) circuit by potential control as shown in Fig. 3a(iii).

A single cell was sealed on the stainless testing chamber loaded with 10 g of coconut coke and placed in a furnace. The stainless testing chamber acted as an anode current collector. Silver foil/wire (Alfa-Aesar) served as a cathode current collector which was adhered onto the LSM layer with a paste of silver ink (99.9%, Alfa-Aesar). The active area for calculation of current density was based on the area of silver paste (1 cm^2) [12].

The Ni/YSZ anode was reduced in H_2 (50 vol% in He) at 800 °C; the cathode was left exposed to air. The SOFC was kept at 800 °C. The V–I curves were measured under flowing He/H_2, He/CO, and He/CO_2 (50/50 vol%; Praxair) at a total flow rate of 100 ml min^{-1}, and He (UHP, Praxair) in 50–1000 ml min^{-1}. Helium served as a carrier gas. The gas flow rates were adjusted by mass flow controllers (Brooks, Model 5850E). The gas stream compositions was varied by (i) a 4-port valve, as shown in Fig. 3b, which produce a step change in concentration and (ii) a 6-port valve which injects 5 cm^3 of CO or CO_2 into the carrier gas stream, producing a pulse change in the concentration of these species.

2.3. Cell characterization

The crystalline phase of anode was characterized by Powder X-ray (XRD) patterns (Philips Analytical X-Ray PW1710) using Cu-Kα radiation at 40 kV and 35 mA with a step size of 0.02° and a scanning rate of 1 s per step.

3. Results and discussion

Fig. 4 shows XRD patterns of fresh NiO/YSZ, H_2-reduced NiO/YSZ and used Ni/YSZ anodes. The pattern of NiO/YSZ shows major diffraction peaks in the presence of NiO (1 1 1) at 36.8°, NiO (2 0 0) at 42.8°, and YSZ peaks at 29.5°, 34.5°, 49.8°, and 59.3°, which were assigned to YSZ (1 1 1), YSZ (2 0 0), YSZ (2 2 0), and YSZ (3 1 1), respectively [13]. H_2-reduced NiO/YSZ shows two diffraction peaks of Ni (1 1 1) at 44° and Ni (2 0 0) at 51.4°, indicating the complete reduction of NiO before cell testing and after exposure of air at room temperature for XRD. The used Ni/YSZ anode produced both NiO and Ni XRD pattern, indicating that coke possesses less reducing capability than H_2 and residual oxygen anion from cathode oxidized Ni to NiO.

Fig. 5 shows the effect of carrier gas flow rates on the voltage–current–power density curves (V–I–P plot) of C-SOFCs at 800 °C. Increasing the flow rate from 50 to 1000 ml min^{-1} decreased OCVs and current densities of C-SOFCs from 0.87 to 0.71 V and from 0.34 to 0.12 A cm^{-2}, respectively. The major gaseous products at a C-SOFC effluent flow rate of 100 ml min^{-1} are 3.8% CO and 1.1% CO_2. The low flow range gave high OCVs and current densities, suggesting that low flow rate increased the residence time of gas-phase species such as carbon monoxide (i.e., CO), which contributed to current generation by electrochemical oxidation:

$$CO + O^{2-} \rightarrow CO_2 + 2e^- \quad (1)$$

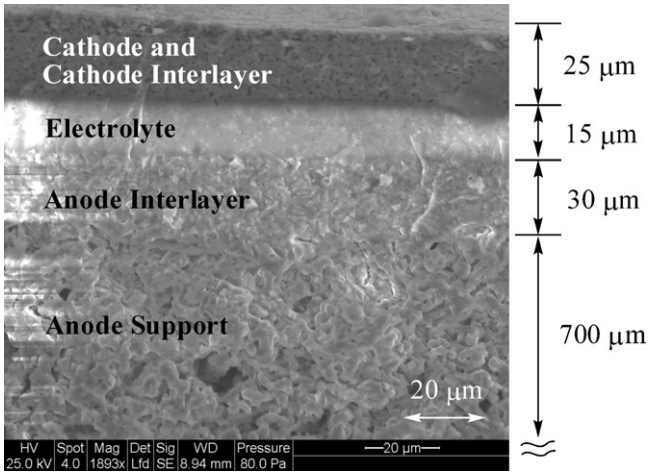

Fig. 2. SEM picture of a SOFC.

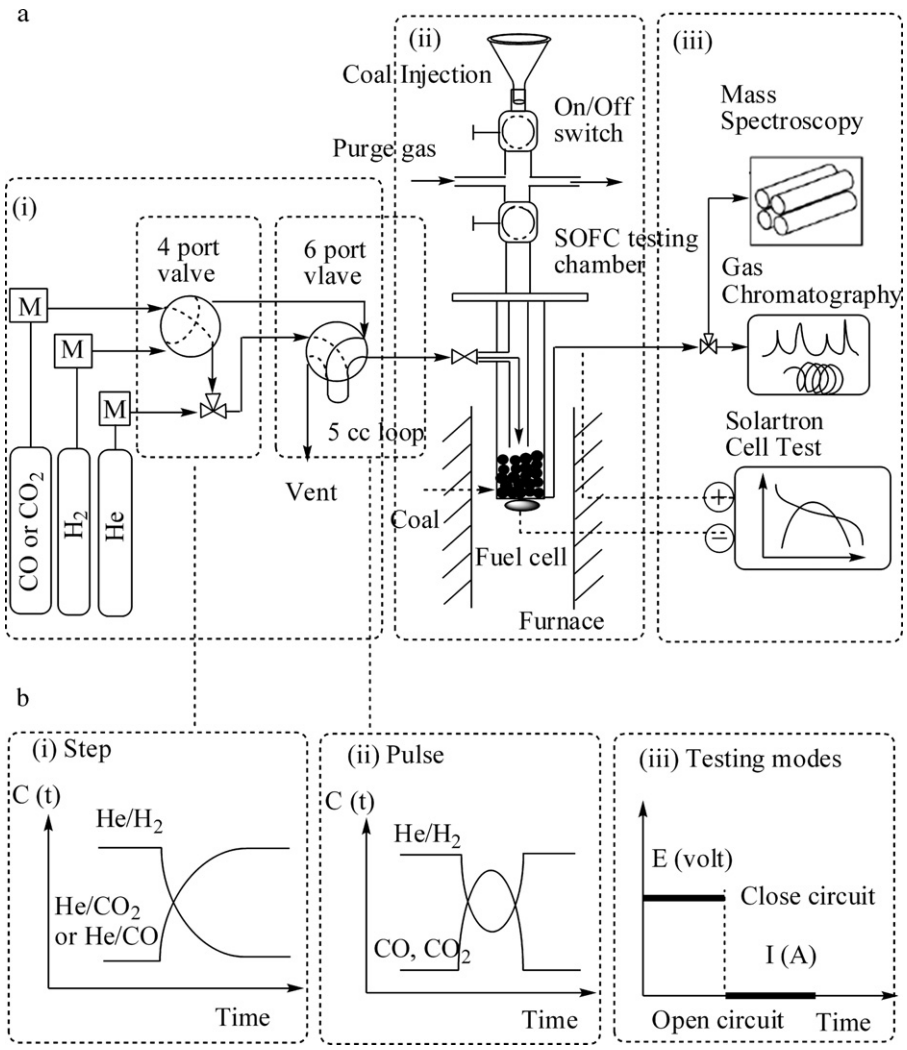

Fig. 3. A schematic of carbon fuel cell testing system and transient techniques.

Current can also be produced from electrochemical oxidation of solid coke to CO and CO_2:

$$C + O^{2-} \rightarrow CO + 2e^- \quad (2)$$

$$C + 2O^{2-} \rightarrow CO_2 + 4e^- \quad (3)$$

The obtained current (I; $C\,s^{-1}$) from C-SOFCs equals to $(n_1r_1 + n_2r_2 + n_3r_3) \times F$, where n_1 (=2), n_2 (=2), and n_3 (=4) are released electrons; r_1, r_2, and r_3 are reaction rates (mol s^{-1}); F is Faraday's constant (96,500 C per mole electron). The contribution of CO electrochemical oxidation (n_1r_1) to current generation (I) at maximum power output was estimated to be 48% at 200 ml min^{-1}, 61% at 100 ml min^{-1}, and 66% at 50 ml min^{-1}, assuming that 100% current was contributed from carbon electrochemical oxidation at

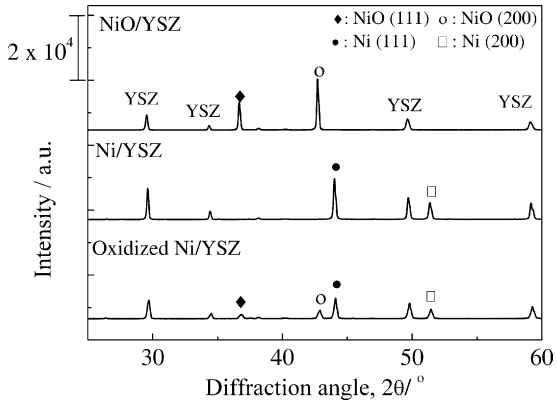

Fig. 4. XRD of NiO/YSZ, Ni/YSZ and used Ni/YSZ.

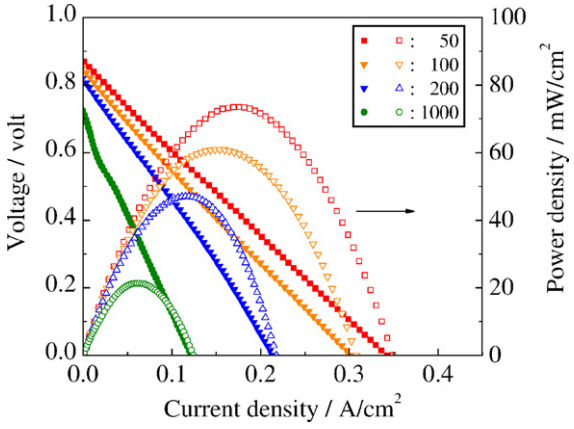

Fig. 5. Voltage–current–power density curves (V–I–P plot) of carbon fuel cells in different flow rates (number denoted; ml min^{-1}) of helium at 800 °C.

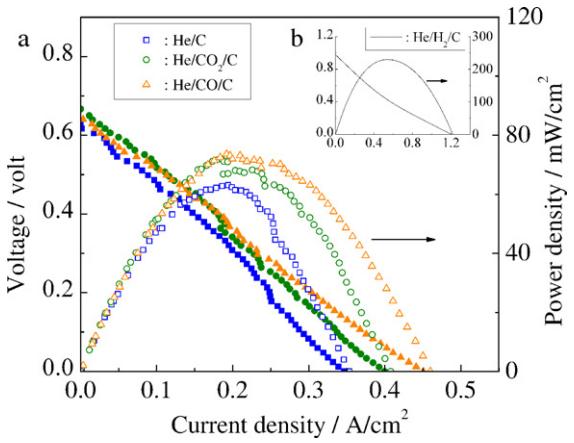

Fig. 6. Voltage–current–power density curves (V–I–P plot) of carbon fuel cells in different gas flows of He/CO_2, He/CO, H_2/He (50/50 vol%; total flow rate: 100 ml min^{-1}) at 800 °C.

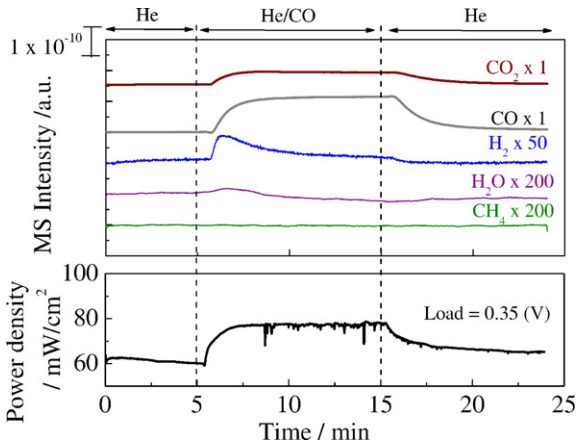

Fig. 8. Power density and MS profiles during introducing a He/CO (50/50 vol%; total flow rate: 100 ml min^{-1}) gas stream on C-SOFCs at 800 °C.

1000 ml min^{-1} where CO_2 and CO were highly diluted by high carrier gas flow rate.

Fig. 6 shows the maximum current density produced by C-SOFCs decreased in the following order: H_2/He > CO/He > CO_2/He > He. The Ni anode is known to be more active in catalyzing H_2 than CO in electrochemical oxidation [14]. The decreasing order of cell performance: CO/He > CO_2/He > He reflects the diminishing role of the contribution of the current (I) produced from CO electrochemical oxidation.

Fig. 7 shows power density and MS profiles resulted from switching the inlet flow from He to He/CO_2. The flow switching produced a step change in CO_2 concentration which caused an immediate overshoot in H_2 and H_2O profiles. The power density increased sharply from 60 to 95 mW cm^{-2} along with CO profile. The power density as well as CO, H_2, and H_2O profiles exhibited a decay trend. The decline in power density can be attributed to the decrease in the concentration of CO, further confirming the contribution of CO electrochemical oxidation to the power generation in C-SOFCs. The declining CO MS profile could be due to gradual depletion of those highly active carbon species for Boudouard reaction. The CO from Boudouard reaction has been reported to have the highest conversion rate initially, followed by a continuous decrease to a steady-state value [15]. The rate of Boudouard reaction is expected to be governed by the reactivity of the active site on carbon surface and diffusion of CO_2 and CO [16,17].

The overshoots of H_2 and H_2O MS profiles leaded that of CO and CO_2, shown in the inset of Fig. 7, indicated that CO/ CO_2 can displace hydrogen in the coke. The H_2 displacement was also observed during the step switching of the flow from He to He/CO, shown in Fig. 8. The parallel trend in CO and power density profile in Fig. 8 further confirm the effectiveness of electrochemical oxidation of CO in current generation.

Fig. 9 shows CO and CO_2 pulse transient studies on C-SOFCs at three different carrier flow rates under OCV condition at 800 °C. Decreasing carrier flow rate increased the OCV and CO MS intensity, revealing that CO was the primary product of electrochemical oxidation of coconut coke. Pulsing CO and CO_2 produced an overshoot of H_2 and OCV, further confirming (i) displacement of hydrogen in coke by CO/CO_2, (ii) occurrence of Boudouard reaction, and (iii) OCV increases due to electrochemical oxidation of CO to CO_2.

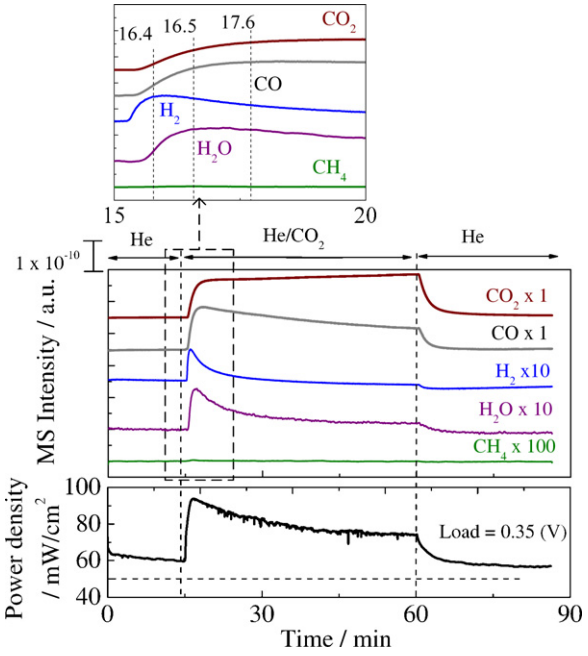

Fig. 7. Power density and MS profiles during introducing a He/CO_2 (50/50 vol%; total flow rate: 100 ml min^{-1}) gas stream on C-SOFCs at 800 °C.

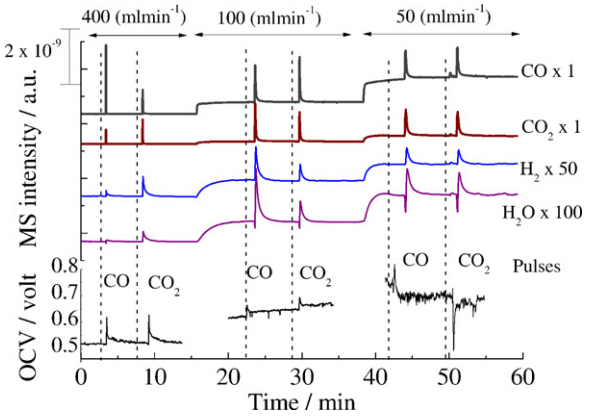

Fig. 9. MS profiles and OCV versus time of C-SOFCs during pulse injection of CO and CO_2 in different helium flow rates at 800 °C.

4. Conclusions

Carrier gas flow rates were found to have a significant effect on the voltage and current produced from C-SOFCs. C-SOFCs operated with coconut coke produced CO as a primary product at 800 °C. In contrast to coke contacting on the surface of the porous Ni/YSZ anode, gaseous CO can diffuse into the porous structure and has an access to TPB in the porous structure. Thus, increasing the concentration of CO by decreasing carrier gas flow rate resulted in enhancing the rate of electrochemical oxidation of CO to CO_2. CO_2 produced can further react with solid fuels via Boudouard reaction to produce CO. The CO and CO_2 pulse transient studies further confirmed the effect of flow rates on fuel cell performance and revealed that CO and CO_2 can displace residual hydrogen in coconut coke fuels.

Acknowledgements

This work was supported by Ohio Coal Development Office (OCDO) (OCRC-C1), Department of Energy (DE-FE0000528), and FirstEnergy Corp. The authors would like to thank Jak Tanthana for tape casting of anodes/electrolyte, Annie Chen and Patrick Mason for lamination and screen-printing of cathode.

References

[1] N.J. Cherepy, R. Krueger, K.J. Fiet, A.F. Jankowski, J.F. Cooper, J. Electrochem. Soc. 152 (2005) A80–A87.
[2] M.J. Antal Jr., G.C. Nihous, Ind. Eng. Chem. Res. 47 (2008) 2442–2448.
[3] J. Michael Jerry Antal, G.r.C. Nihous, Ind. Eng. Chem. Res. 47 (2008) 2442–2448.
[4] T. Nunoura, K. Dowaki, C. Fushimi, S. Allen, E. Meĭszaĭros, J. Michael Jerry Antal, Ind. Eng. Chem. Res. 46 (2007) 734–744.
[5] T. Nunoura, K. Dowaki, C. Fushimi, S. Allen, E. Meszaros, M.J. Antal Jr., Ind. Eng. Chem. Res. 46 (2007) 734–744.
[6] S. Li, A.C. Lee, R.E. Mitchell, T.M. Gur, Solid State Ionics 179 (2008) 1549–1552.
[7] R. Liu, C. Zhao, J. Li, F. Zeng, S. Wang, T. Wen, Z. Wen, J. Power Sources 195 (2010) 480–482.
[8] Y. Nabae, K.D. Pointon, J.T.S. Irvine, J. Electrochem. Soc. 156 (2009) B716–B720.
[9] L. Jia, Y. Tian, Q. Liu, C. Xia, J. Yu, Z. Wang, Y. Zhao, Y. Li, J. Power Sources 195 (2010) 5581–5586.
[10] T.M. Gür, M. Homel, A.V. Virkar, J. Power Sources 195 (2010) 1085–1090.
[11] C. Li, Y. Shi, N. Cai, J. Power Sources 195 (2010) 4660–4666.
[12] S.P. Jiang, J.G. Love, L. Apateanu, Solid State Ionics 160 (2003) 15–26.
[13] H. Mohebbi, T. Ebadzadeh, F.A. Hesari, Powder Technol. 188 (2009) 183–186.
[14] Y. Jiang, A.V. Virkar, J. Electrochem. Soc. 150 (2003) A942–A951.
[15] S. Yoshida, J. Matsunami, Y. Hosokawa, O. Yokota, Y. Tamaura, M. Kitamura, Energy Fuels 13 (1999) 961–964.
[16] X. Li, Z.H. Zhu, R. De Marco, A. Dicks, J. Bradley, S. Liu, G.Q. Lu, Ind. Eng. Chem. Res. 47 (2008) 9670–9677.
[17] X. Li, Z. Zhu, R. De Marco, J. Bradley, A. Dicks, J. Power Sources 195 (2010) 4051–4058.